Tunneling spectroscopy in barrier-separated two-dimensional electron-gas systems

W. Demmerle, J. Smoliner, G. Berthold, E. Gornik, and G. Weimann
Walter Schottky Institut, Technische Universität München, Am Coulombwall, D-8046 Garching, Federal Republic of Germany

W. Schlapp
Forschungsinstitut der Deutschen Bundespost, Am Kavalleriesand 3, D-6100 Darmstadt, Federal Republic of Germany
(Received 21 January 1991)

Tunneling processes between subbands in two independently contacted two-dimensional electron-gas systems on a GaAs-$Al_xGa_{1-x}As$-GaAs heterostructure were investigated. The theoretical results obtained by self-consistent calculations are in excellent agreement with the values for the subband energies determined by tunneling spectroscopy. If a magnetic field is applied perpendicular to the planes of the sample, additional structures in the derivative of the current-voltage characteristics are identified as tunneling processes between different Landau levels on both sides of the barrier. With in-plane magnetic fields, the conservation of the canonical momentum results in a very large broadening of the subband resonances. As a consequence, the mean values of the wave functions, even for unoccupied subbands, can be directly determined.

I. INTRODUCTION

The experimental observation of the tunneling effect is, besides diffraction and scattering experiments, a further manifestation of the wave-particle dualism of matter—and of the formalism of quantum mechanics in general. Appropriate systems for such experiments are those of dimensions comparable to the de Broglie wavelength of the tunneling particles. For this reason, charge carriers in semiconductor bulk materials are ideal for the observation of the predictions of quantum mechanics. The spatial dimensions required in such materials were achieved for the first time experimentally in the case of the tunnel diode.[1] By additional vertical structuring, a quantum size effect, a surface bound state of electrons localized in a narrow accumulation layer at an InAs–InAs-oxide interface, was directly observed using electron tunneling.[2,3] In this case, the electric field associated with the surface layer is sufficiently strong to quantize the energy due to the carriers' motion normal to the interface into discrete levels. Structures in the dI/dV vs V and in the d^2I/dV^2 vs V characteristics reflect the energy minima of the two-dimensional electric subbands. Theoretically, it was shown that the tunnel conductance caused by electrons of the nth subband is proportional to the density of states in this subband, which has been referred to as a space-charge-induced localized state.[4] Therefore, these structures are due to the electrons tunneling *resonantly* from a three-dimensional (3D) electrode to the two-dimensional (2D) electron system located at the interface. This means that the total energy, as well as the parallel (to the interface) momentum of the tunneling electrons, is conserved. Tunneling studies at the Si-SiO_2 interface were used to investigate the influence of the electron concentration on the subband occupation in the two-dimensional electron gas (2D EG).[5]

Another method used for vertical structuring is the growing of heterostructures by molecular beam epitaxy or related techniques. This kind of material is most frequently used to study tunneling processes in semiconductors. The well-known experiment on an (n^+-type GaAs)/$Al_xGa_{1-x}As$/GaAs/$Al_xGa_{1-x}As$/(n^+-type GaAs) heterostructure, representing a double-barrier structure for tunneling electrons,[6] was the first of a great number of tunneling experiments. Because of the conservation of both the total energy and the momentum of the electrons parallel to the interfaces, electrons can tunnel resonantly as long as the energy of the quasi-bound state (of the two-dimensional quantum well—intermediate GaAs layer) is located between the Fermi level and the conduction-band edge of the "emitter" electrode (one of the outer n^+-type GaAs layers). Most recently, resonant tunneling of electrons from a 3D metal contact into quantum wires was used to determine the energy spacings of the one-dimensional subbands.[7]

By now, resonant tunneling is a well-studied topic in semiconductor physics.[8] However, there is a scarcity of experiments on structures where the emitter—as well as the collector—electrode are of two-dimensional character. Drastic changes in the $I(V_b)$ characteristics are to be expected due to the conservation of energy and momentum. To the knowledge of the authors, there are only a few published works on this subject. One possibility to realize such a structure is the use of a triple-barrier configuration.[9] In such experiments, however, it is not clear how much of the applied bias voltage drops across the various barriers, and consequently any determination of the energy levels is difficult. Another method is to apply hydrostatic pressure (above 8 kbar) to an AlAs-GaAs-AlAs heterostructure. This switches the heterostructure type II and thus two 2D EG's are formed at the X point of the AlAs layers.[10]

We have studied tunneling processes between two independently contacted 2D EG systems, namely, between an inversion layer and an accumulation layer which are separated by a barrier of 195 Å. By applying a bias voltage V_b to the sample, the quantized states on both sides of the barrier can be shifted energetically by eV_b with respect to each other. Transitions between different subbands are directly observed in the tunneling current $I(V_b)$ and are more clearly seen by taking the derivative dI/dV_b. These resonances are used to determine the subband energies in the accumulation and the inversion channel by comparing the measured results to those obtained by self-consistent calculations. In addition, the influence of a backgate voltage is investigated in the dark as well as after short illumination.

Moreover, if a magnetic field is applied perpendicular to the sample, additional peaks are resolved in dI/dV_b. It is demonstrated that these structures are due to transitions from a Landau level on one side of the barrier to another Landau level on the other side of the barrier, not necessarily with the same quantum number.[11] In order to investigate the momentum conservation rules, the magnetic field is applied parallel to the layers of the sample. A very large broadening of the subband resonances is observed, from which the conservation of the canonical momentum and the conservation of parallel momentum $\mathbf{k}_{\|}$ in the case of zero magnetic field is deduced.[12,13]

The next section gives a description of the sample, the sample preparation and a discussion of the tunneling current measurements, including the results of self-consistent calculations. Subsequently, the results of the experiments where a magnetic field is applied perpendicular (Sec. III) and parallel (Sec. IV) to the layers of the sample are discussed.

II. TUNNELING MEASUREMENTS

The sample consists of a nominally undoped GaAs layer ($N_A \leq 1\times10^{15}$ cm^{-3}) grown on a semi-insulating substrate, followed by an undoped spacer ($d = 50$ Å), doped $Al_xGa_{1-x}As$ ($d = 45$ Å, $N_D = 4\times10^{18}$ cm^{-3}, $x = 0.36$), another spacer ($d = 100$ Å) and n^--type doped GaAs ($d = 800$ Å, $N_D = 1.2\times10^{15}$ cm^{-3}). An additional GaAs cap layer was highly n-type doped ($d = 150$ Å, $N_D = 6.4\times10^{18}$ cm^{-3}). The resulting band structure is shown in Fig. 1(a), where the inversion layer and the accumulation layer are separated by only 195 Å. From Shubnikov–de Haas (SdH) measurements on sample No. 1 it was deduced that in both the inversion layer and the accumulation layer only one subband is occupied having electron concentrations of $n_s^{inv} = 6.3\times10^{11}$ cm^{-2} and $n_s^{acc} = 5.8\times10^{11}$ cm^{-2}, respectively. The contacts to the inversion layer were formed using a Au/Au-Ge/Ni alloy. For an Ohmic contact to the upper channel (accumulation layer) Au-Ge was used, too, but in this case the Au-Ge was only slightly diffused into the n^--type doped GaAs. The upper GaAs layers around the top contact were removed selectively in order to locally deplete the accumulation channel. This preparation technique leads to independent contacts to both electron gas systems, as can be seen in Fig. 1(b). The dotted line shows the current path: in the case of a positive bias voltage the electrons enter the system via the two outer contacts, thermalize in the inversion channel, and move to the middle of the sample. They then tunnel through the $Al_xGa_{1-x}As$ barrier into the accumulation layer and leave the system via the top contact.

All measurements of the current-voltage characteristic $I(V_b)$ and its derivative dI/dV_b were made using a four-terminal conductance bridge[14] in order to compensate series resistances inside the contacts and the inversion channel. The modulation frequency of 22 Hz and modulation voltage of 0.3 mV were chosen to achieve a high resolution and to avoid parasitical capacitive perturbations.

Figure 2 shows the current-voltage characteristic $I(V_b)$ and its derivative dI/dV_b for sample No. 1, measured at a temperature of 4.2 K. Several steplike structures in $I(V_b)$ are clearly observed, most clearly at bias voltages of $V_b = +2.2$ and -32.5 mV. At more negative bias voltages, the $I(V_b)$ characteristic shows only a few very weak structures which are only clearly seen in the derivative signal as a series of sharp peaks.

To understand these characteristics, one has to bear in mind that the samples are provided with two independently contacted 2D EG's. The total energy of an electron in a 2D EG system can be written as $E = E_\perp + E_{\|}$,

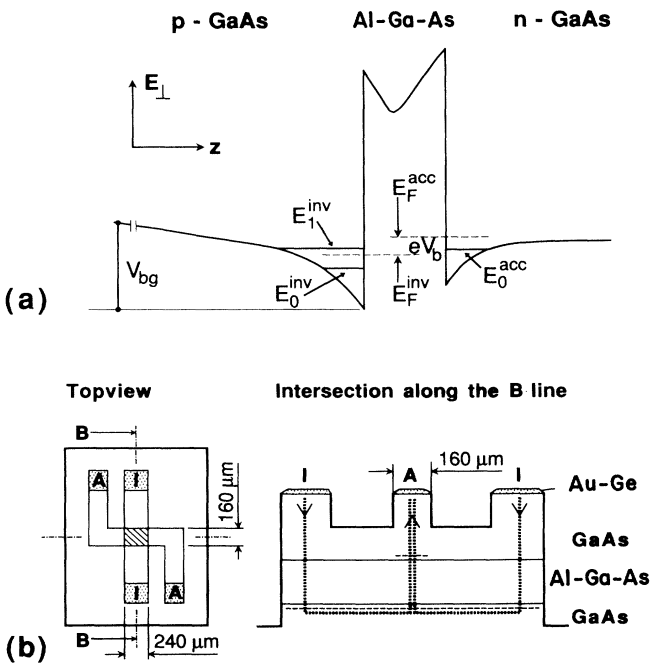

FIG. 1. (a) Band structure of a typical sample. E_0^{acc} and E_n^{inv} denote the subbands in the accumulation and inversion layers. E_F^{acc} and E_F^{inv} are the corresponding Fermi levels. V_b stands for the applied bias voltage, V_{bg} for the backgate voltage. (b) Top view and intersection along the B line after sample preparation: **I** and **A** denote the contacts to the inversion layer and the accumulation layer, respectively. The dotted line indicates the current path, assuming a positive bias voltage.

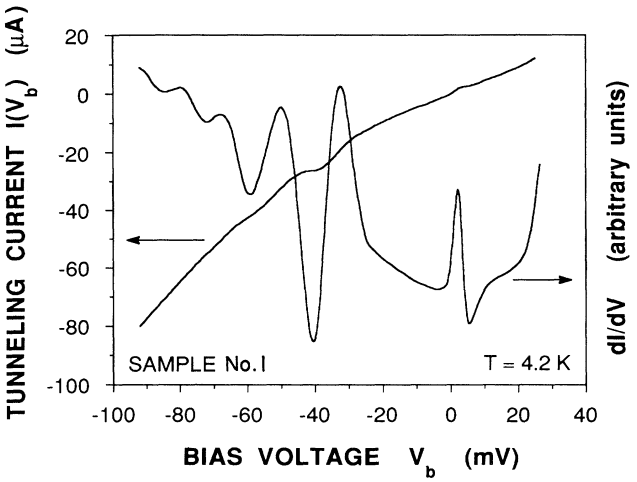

FIG. 2. Current-voltage characteristics $I(V_b)$ of sample No. 1, measured at $T = 4.2$ K, and its derivative, dI/dV_b.

where $E_\perp$ corresponds to the electrons' energy at the subband edge. The energy of the carriers' motion parallel to the channel is denoted by $E_\parallel = \hbar^2\mathbf{k}_\parallel^2/2m^* = \hbar^2k_x^2/2m^* + \hbar^2k_y^2/2m^*$ (in case the z direction is parallel to the growth axis). As the translational symmetry is retained in the x and y direction, these coordinates are cyclic, and therefore $\mathbf{k}_\parallel$ and $E_\parallel$ should be conserved. By applying a bias voltage V_b to the sample, where in the ideal case the voltage drops exclusively over the barrier, it is possible to shift both 2D EG systems energetically with respect to each other. Resonances between the two quantized systems occur when a subband edge in the accumulation channel $E_m^{\rm acc}$ becomes degenerate with one in the inversion channel ($E_n^{\rm inv}$), again assuming that $\mathbf{k}_\parallel$ is conserved in the tunneling process. $E_\parallel$ should have no influence on the tunneling current. Thus, the peak in dI/dV_b at $V_b = +2.2$ mV (inversion layer grounded) is attributed to the tunneling process from $E_0^{\rm inv}$ into the lowest subband in the accumulation layer, $E_0^{\rm acc}$, which will be referred to as the 0-0 transition. At higher positive bias voltages no further peaks can be observed in dI/dV_b and thus we conclude that there is only one subband in the accumulation layer. Consequently, the first peak in dI/dV_b at a negative bias of $V_b = -32.5$ mV is due to a tunneling process from $E_0^{\rm acc}$ into $E_1^{\rm inv}$ (0-1 transition). The subsequent peaks correspond to transitions into higher subbands. Although these structures soon become less pronounced with increasing negative voltage due to the large current flowing through the sample, up to eight subbands are observed.

It will be shown later that, to a very good approximation, the applied bias voltage V_b drops entirely across the barrier, i.e., results in an energetic shift $\Delta E = eV_b$ of the two 2D EG systems with respect to each other. Therefore, the differences in bias voltage between the resonance peak for the 0-0 transition and the 0-n transition give directly the subband spacings in the inversion channel. This is not immediately obvious due to the self-consistent nature of the band structure, since the change in the bias voltage causes a change in the electron concentrations in both the inversion and the accumulation layer.

The width of the resonance in the current-voltage characteristic can be readily obtained by measuring the linewidth of the peaks in dI/dV_b, giving values of around 10 meV. As the liquid-helium temperature corresponds to an energy of $k_BT = 0.36$ meV, thermal broadening cannot be responsible for the observed values. However, the resonance range is expected to depend on the full linewidth of a resonant peak in the coherent transmission probability, ΔE_T. On the other hand, ΔE_T and the tunneling lifetime of the quasilevel giving rise to the resonance, τ, are necessarily related by $\Delta E_T = \hbar/\tau$ (Ref. 15). Within a simple model, the time τ can be estimated by $\tau^{-1} = [(\hbar k/m^*)/2b]D_T$, where k is the wave vector of the tunneling electron, b is the width of the potential the electron is confined by and D_T is the transmission probability through the barrier.[16] For realistic values ($b = 120$ Å, $k = 3.0 \times 10^8$ m^{-1}), assuming ideal transmission ($D_T = 1$), an upper limit $\Delta E_T \leq 14$ meV for the energy uncertainty is obtained. Therefore, the linewidths of the resonance structures observed in dI/dV_b are within the same range as the results predicted by a simple theory of resonant tunneling.

The carrier concentrations at zero bias both in the accumulation and the inversion layer, are equivalent to a Fermi energy of about $E_F \approx 20$ meV. If the momentum of the electrons parallel to the interfaces was not conserved, the width of the resonance structure in dI/dV_b (i.e., the linewidth of the peaks) would be expected to be in the same order as the Fermi energy, just as in the case of the double-barrier structure mentioned above, where electrons tunnel from a 3D "emitter" electrode into a 2D quantum well. But since much smaller values for the linewidth are obtained from the experimental data, the assumption of $\mathbf{k}_\parallel$ conservation is justified. Consequently, the resonance condition is given by

$$E_n^{\rm inv} = E_0^{\rm acc}. \tag{1}$$

Nevertheless, there is a slight inconsistency between the results obtained by the experiment and the theoretical predictions. As discussed above, in the ideal case tunneling between the two 2D systems is expected to occur at well-defined bias voltages provided by the resonance condition (1) to satisfy the conservation of total energy and parallel momentum. If the two quantum states were misaligned energetically (i.e., in $E_\perp$), resonant tunneling would *not* be allowed at all, resulting in a clear decrease of the current or in large negative differential resistances in dI/dV_b. The measured current-voltage characteristic shows such a behavior only very weakly for the 0-0 and the 0-1 transitions, whereas with increasing negative bias voltage the current grows exponentially. This large current background, on which the structures due to the subband resonances are superimposed, is caused by electrons tunneling nonresonantly, i.e., without conservation of total energy and parallel momentum through the barrier. The annihilation of the momentum and energy information of a tunneling electron is mainly due to scattering

inside the highly doped $Al_xGa_{1-x}As$ barrier which becomes dominant at high negative bias voltages. Therefore, the form of the resonance structures in $I(V_b)$ can be understood as a superposition of two current contributions. One is caused by electrons tunneling resonantly through the barrier, which results in a peak-shaped current, and the other is caused by electrons tunneling nonresonantly which gives an exponential current behavior. The latter is especially dominant at high negative bias.

Backgate voltage effects

By applying a backgate voltage V_{bg} between the inversion layer (grounded) and the back of the sample, as indicated in Fig. 1(a), the strength of the electric field and therefore the potential distribution at the lower GaAs-$Al_xGa_{1-x}As$ interface can be influenced. This results in a change of the subband energies as well as of the electron concentration in the 2D EG. The experimental results for sample No. 1 are shown in Fig. 3, where we have plotted the dI/dV_b characteristics for both positive and negative backgate voltages. In the case of a positive backgate voltage the resonance peak of the 0-0 transition remains almost unaffected, whereas the peaks of the higher transitions clearly shift to lower (negative) bias voltages and are washed out drastically as V_{bg} increases. The position of the peak in dI/dV_b that corresponds to the 0-1 transition starts to saturate at backgate voltages higher than $V_{bg} = +150$ V. The resonance structure of the 0-2 transition also shows such a saturation behavior for $V_{bg} > +250$ V, although more weakly, whereas the peaks in dI/dV_b of all higher transitions become completely unresolved at high backgate voltages. Within a simple capacitor model, a positive backgate voltage lowers the electric field at the GaAs-$Al_xGa_{1-x}As$ interface. In addition, the electron concentration of the inversion channel is increased. Hence, a decrease of the energy differences between the subbands is expected, resulting in a shift of the resonance peaks in dI/dV_b to lower bias voltages. In contrast to that, the steepness of the potential on the GaAs side of the interface is increased for $V_{bg} < 0$ due to the larger electric field. This should lead to larger subband spacings in the inversion layer. In the experiment, this behavior results in a shift of all resonance structures in dI/dV_b to more negative bias voltages (Fig. 3), which is more pronounced for the 0-1 and higher transitions than for the 0-0 transiton. In addition, the peak intensities and the linewidths rise with increasing negative backgate voltage.

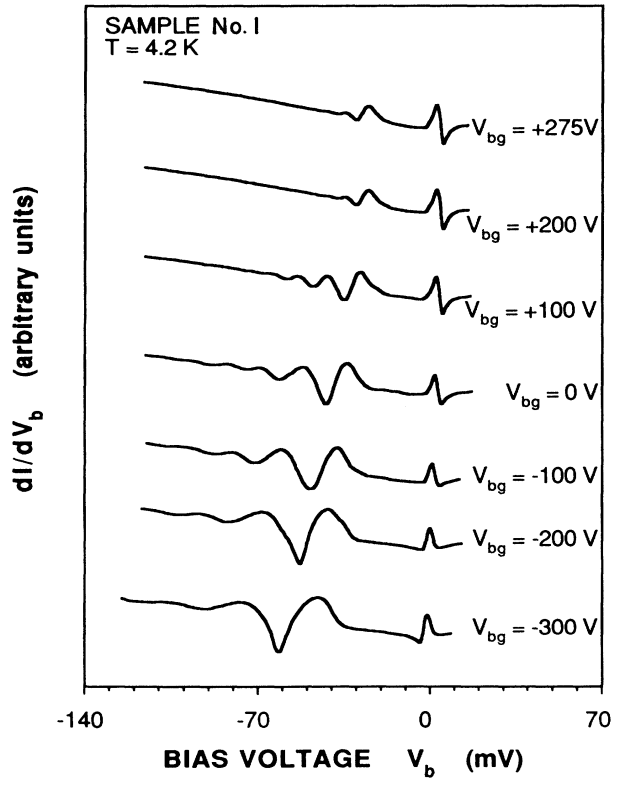

FIG. 3. dI/dV_b curves for sample No. 1 at various backgate voltages. All curves are scaled to fit on the same plot.

Self-consistent calculations, similar to those carried out by Stern and Das Sarma,[17] were performed in order to determine the positions of the subband resonances. To determine these resonance peak positions, the energy levels in both channels were calculated as a function of the carrier concentrations. The Numerov algorithm is used to solve the Schrödinger equation numerically, where the influence of the Hartree potential and doping effects, as well as corrections due to exchange and correlation[18] and due to nonparabolicity,[19] are included. For the conduction-band discontinuity a value of $\Delta E_c/\Delta E_g = 0.61$ is used.[20] Due to the small difference in the dielectric constants, image-force effects are very small in GaAs-$Al_xGa_{1-x}As$ heterostructures, and are neglected. As all measurements have been carried out at low temperatures ($T = 4.2$ K), we assume an absolute zero Fermi-Dirac distribution function. The only fitting parameter used is the depletion charge n_d, as done in previous work.[21] This is justified by the uncertain value of the acceptor concentration in the GaAs buffer layer. The additional electric field at the lower GaAs-$Al_xGa_{1-x}As$ interface, caused by the external field due to an applied backgate voltage, was treated as a change in the depletion charge by

$$\Delta n_d = -\epsilon_0 \epsilon_r V_{bg}/e d_s, \tag{2}$$

where d_s denotes the sample thickness and $\epsilon_0\epsilon_r$ the dielectric constant of GaAs.

The theoretical results for zero applied backgate voltage are shown in Fig. 4. The best agreement between theory and experiment was achieved with $n_d = 1.32 \times 10^{11}$ cm^{-2}. All subband energies in the inversion layer (full lines) show only a weak, nearly linear dependence on the applied voltage, the energy spacings of the subbands remaining almost constant. This result shows the dominant influence of the depletion field on the energy levels in the 2D EG. However, the subband in the accumulation channel (broken line) is strongly affected by the bias voltage, because the potential at the upper $Al_xGa_{1-x}As$-GaAs interfaces is exclusively determined by the electron

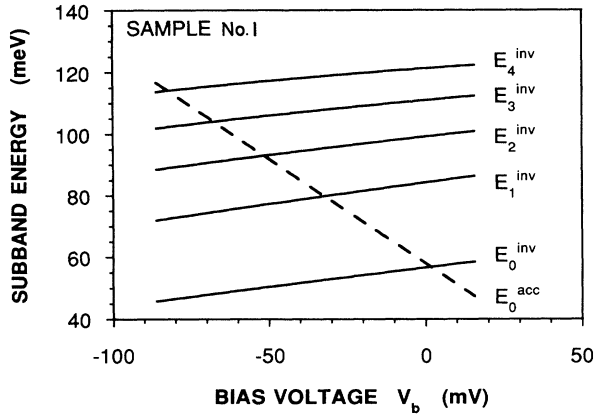

FIG. 4. Calculated subband energies both of the inversion layer (full lines) and the accumulation layer (broken line) for zero applied backgate voltage. Resonant tunneling occurs each time the subband E_0^{acc} matches a subband E_n^{inv}.

charge itself. The points where the broken and solid lines cross denote the bias voltages at which resonant tunneling is allowed. Therefore, Fig. 4 also shows that the differences in bias voltage $e\Delta V_b$ between two resonant tunneling peaks in dI/dV_b are in good agreement with the subband energy spacings in the inversion layer.

To analyze the influence of an applied backgate voltage, the experimental data and the results obtained by the calculation are compared in Fig. 5, where the differences in the resonance peak positions are plotted versus the backgate voltage for sample No. 1. E_{0n} denotes the difference in bias voltage between the resonance peak for the 0-0 transition and the peak for the 0-n transition. The results obtained by the calculations (full lines) are in excellent agreement with the experimental data. Note that the experimentally observed saturation of the peak positions at high positive backgate voltages is also reproduced by the calculations.

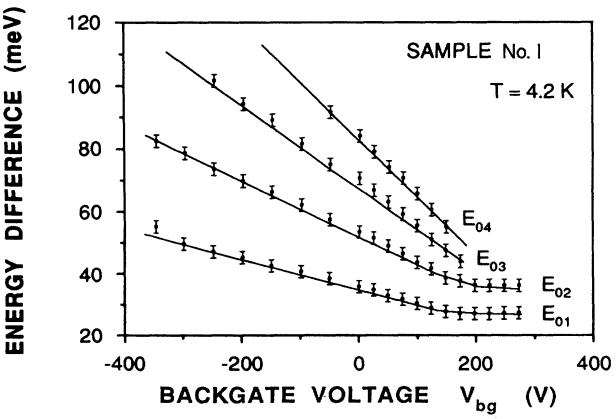

FIG. 5. Comparison between theoretical data (full lines) and experimental data (dots, including error bars) as a function of the applied backgate voltage for sample No. 1. E_{0n} denotes the difference in bias voltage between the resonance peak for the 0-0 transition and the 0-n transition.

As mentioned above, the condition $V_{bg} > 0$ is simulated by a decrease in either the depletion charge or field at the lower GaAs-$Al_xGa_{1-x}As$ interface. This lessens the confinement of electrons at this interface, and consequently should reduce the energies of the subbands and their spacing. However, the electric field at the interface is mainly determined by the Hartree potential, as the electrons in the ground state are confined very close to the interface. For this reason, the energies of the lower subbands in the inversion channel are only affected by an increasing backgate voltage if the depletion field contributes more to the confinement potential than the Hartree term. This explains why the position of the resonance peak of the 0-0 transition shows no dependence on positive V_{bg}, while the corresponding peak positions for the 0-1 and the 0-2 transitions start to saturate at backgate voltages higher than $V_{bg} = +150$ and $+250$ V, respectively. As the energies of the higher subbands are mainly influenced by the depletion field, an increase of $+V_{bg}$ results in a rapid decrease of the energy separation and finally in a total vanishing of the subbands. Therefore, in the experimental data the resonance structures in dI/dV_b of the transitions into higher subbands of the inversion channel first become weaker and then disappear as the positive backgate voltage is increased.

In analogy, the case of $V_{bg} < 0$ V is modeled by an additional amount of depletion charge which enhances the confining electric field at the interface. This leads to an increase of the subband energies, as well as subband spacings, in the inversion layer. This reproduces the observed shift of the resonance peaks in dI/dV_b to more negative bias voltages. For the reasons described above the influence of the negative backgate voltage is stronger on the higher subbands. This effect is seen in the experimental data: the shift of the 0-2 transition peak is larger than that of the 0-1 peak. Finally, the observed enhancement of the resonance structures for the 0-1 and higher transitions at high negative backgate voltages can be explained by the better confinement under these circumstances.

In summary, the excellent agreement between theory and experiment obtained by tunneling spectroscopy at both positive and negative backgate voltages justifies the assumptions made in our model. It was also shown that the subband energies and their spacings can be tuned over a wide range by the applying of an external backgate voltage to the sample. For example, the spacing between the ground state and the first excited subband in the inversion channel can be tuned between 25 and 40 meV. However, the most important conclusion to be drawn from these results is that to a very good approximation the quantized states of the two 2D EG systems are shifted by $\Delta E = eV_b$ with respect to each other when a bias voltage V_b is applied to the junction.

Hence, such a heterostructure is ideally suited to study the influence of various boundary conditions on the tunneling process between the quantized states of the two 2D EG systems.

In a further study, tunneling measurements were carried out after brief illumination. For that purpose, sample No. 1, which has a semitransparent top contact,

was illuminated by a red light-emitting diode (LED) for about 4 sec. The high-frequency tail of the LED's emission spectrum is of sufficient energy to excite across the GaAs fundamental gap. Figure 6 shows the measured dI/dV_b characteristics after illumination for various backgate voltages. In comparison to Fig. 3, all resonance peaks are shifted towards zero bias voltage. The basic behavior of the resonances, however, is not changed if a negative backgate voltage is applied to the sample. Note that in the case of $V_{bg} > 0$ the peak positions shift only slightly with an increasing backgate voltage, whereas the peaks of the transitions into higher subbands become smaller and vanish above $V_{bg} = +250$ V.

As a result of the illumination, acceptor levels in the residual p-type doped GaAs layer are ionized and the electrons are lifted into the conduction band. As a consequence, the electron concentration of the inversion channel is increased by $\Delta n_s^{inv} = 0.5 \times 10^{11}$ cm^{-2}, as obtained from SdH measurements. Again, self-consistent calculations are performed, once more using the depletion charge as the only fitting parameter, leading to a value of $n_d^{illum} = 0.47 \times 10^{11}$ cm^{-2}, which is very similar to Δn_s^{inv}. The difference between n_d and n_d^{illum} corresponds to a virtual backgate voltage of $V_{bg}^{illum} \approx +240$ V, according to Eq. (2). This explains that there is no additional shift of the resonance peaks in the case of a positive backgate voltage—the saturation effect starts already at $V_{bg} = +0$ V.

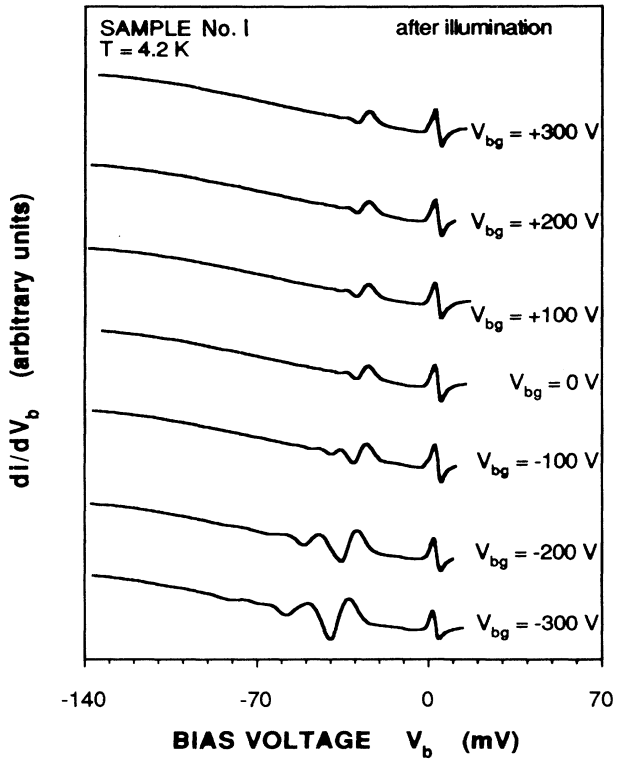

FIG. 6. dI/dV_b curves for sample No. 1 at various backgate voltages, measured after brief illumination. All curves are scaled to fit on the same plot.

These experimental results do not change if the sample is illuminated again or for a longer time. Therefore, we conclude that it is not possible to entirely reduce the depletion charge by illumination. Further, the excellent agreement between theory and experiment emphasizes the close relation between depletion charge and backgate voltage, as first assumed in Eq. (2).

III. TUNNELING PROCESSES IN PERPENDICULAR MAGNETIC FIELDS

In this section, the tunneling current is studied as a function of a magnetic field applied perpendicular to the two 2D EG's. The additional potential contribution due to the magnetic field causes $E_{\parallel}$ to be quantized into Landau levels.

In 1970, Tsui[2,3] investigated the Landau-level spectra of electrons in the electric subbands of a narrow accumulation layer using tunneling spectroscopy. Oscillations in the second derivative of the tunneling current were observed as a result of the magnetic field and give a direct measure of the in-plane effective mass of the confined electrons. Since then, many magneto-tunneling experiments have been performed on single-barrier[22] and double-barrier GaAs-$Al_xGa_{1-x}As$ heterostructures.[23,24] In the latter case, resonant tunneling of electrons through Landau levels inside the well was observed. Similar results are obtained on $In_xGa_{1-x}As$-InP systems.[25] Common to most of these experiments is the fact that electrons tunnel from a metal contact or a highly n-type doped electrode into a 2D EG system. As the electron scattering rates in these types of emitter electrodes are high, well-resolved Laudau quantization only exist inside the 2D EG's. An alignment of the Fermi level in the emitter with the various Landau levels of each electronic subband in the 2D EG causes a series of oscillations in d^2I/dV^2. Most recently, Kane, Tsui, and Weimann[26] found evidence of inter-Landau-level tunneling in a 2D EG between regions of different electron densities induced by a front gate contact. When a magnetic field was applied, the current between the two regions showed a backward pn-diode-like behavior. Treating the Landau-level separation at the boundary of these regions similarly to the semiconductor band gap in a backward diode, the existence of inter-Landau-level tunneling was used to explain the current flow at reverse bias. Nevertheless, disorder in the transition region had to be assumed in order to introduce a coupling between Landau levels and thus allow tunneling to occur.

In our sample the situation is somewhat different as well-defined Landau levels exist in both the inversion channel and the accumulation channel, which are only 195 Å apart. The existence of several subbands in the inversion channel further complicates the situation. The total energy of an electron, for instance, in the inversion layer, is therefore given by two quantum numbers, the subband index n and the Landau-level index N, and can be written as $E = E_{n,N}^{inv} = E_n^{inv} + \hbar\omega_c(N + \frac{1}{2})$. If an electron that tunnels from the inversion channel into the accumulation channel suffers no scattering during the tunneling process, the momentum and energy information

is conserved. Thus, conservation of Landau-level index N is expected. Note that, if the applied bias voltage adjusts two subbands energetically according to the resonance condition (1), all Landau levels on both sides of the barrier will be aligned automatically, as their spacing $\hbar\omega_c$ is solely determined by the magnetic field. Shifting the quantized systems energetically with respect to each other by an amount of $N\hbar\omega_c$, a state is created where a Landau level in the accumulation layer is degenerate with a Landau level in the inversion channel. In such a tunneling process between two states of different Landau index, resonant tunneling is not allowed in the absence of scattering. Thus, no additional resonance structures are expected in the tunneling current.

Figure 7 shows the derivatives dI/dV_b of the current-voltage characteristics at various values of a magnetic field for sample No. 2. At field strengths below $B = 3$ T, only the zero-field resonant transitions can be observed. For higher fields, however, additional structures, marked by arrows, are clearly revealed in dI/dV_b on both sides of the resonance peak corresponding to the 0-0 transition. The position of the $B = 0$ T resonance does not change with increasing magnetic field. The additional peaks on the left and on the right side of it are shifted to more negative and more positive bias voltages, respectively. Simultaneously, the linewidths and the amplitudes of these peaks, as well as their distances, grow larger. The peaks vanish whenever they approach the next-highest subband resonance position. For the 0-1 transition, a similar behavior could not be resolved. At magnetic fields higher than $B = 6$ T, the measurements are more and more disturbed by the occurrence of a Hall voltage V_H, arising from the the current in the inversion channel flowing perpendicular to the magnetic field direction. In this case, a serious analysis of the experimental results was not attempted.

In Fig. 8(a), the bias voltages at the marked peaks in Fig. 7 are plotted versus the applied magnetic field.

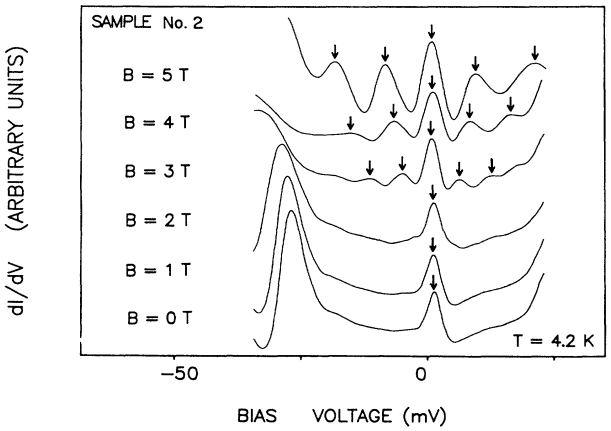

FIG. 7. Selected dI/dV_b curves for different magnetic fields applied perpendicular to the 2D EG's. The 0-0 transition as well as the corresponding additional structures are marked by arrows.

The peak positions vary linearly with the magnetic field B and at any given field are equally spaced. In addition, lines are drawn into the fan chart with gradients of $\pm\hbar\omega_c/B$ and $\pm 2\hbar\omega_c/B$. Thereby, the effective mass is used as a fitting parameter, leading to a best fit value of $m^*/m_0 = 0.067 \pm 0.005$. As all structures appear at distances from the $B = 0$ T resonance equal to integer multiples of the cyclotron energy $\hbar\omega_c/e$, the additional peaks in dI/dV_b are interpreted as tunneling processes between Landau levels on both sides of the barrier with different Landau-level index. The numbers at the end of the lines in Fig. 8(a) denote the change in the Landau-level index ΔN. The result is a proof that the bias voltage drops completely across the barrier, since the effective mass obtained is very close to the free-electron mass of GaAs.

According to the theoretical predictions, transitions

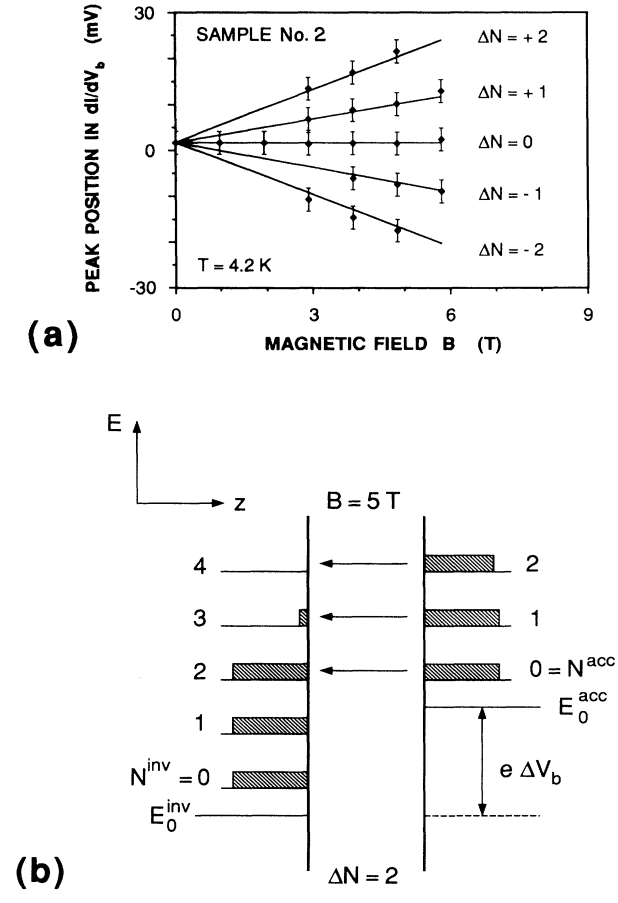

FIG. 8. (a) Fan chart of the observed peak positions vs magnetic field. The numbers at the end of the lines denote the change in Landau-level index ΔN. (b) Tunneling processes, corresponding to the 0-0 transition, are illustrated schematically for $B = 5$ T at reverse bias. The Landau-level index is changed by $\Delta N = 2$. ΔV_b denotes the shift in bias voltage compared to the zero-field resonance position to achieve a new resonance condition. The target level must not be completely occupied.

between Landau levels with different indices are only possible if the electron momentum is changed during the tunneling process. Since at zero magnetic field the tunneling current is independent of $E_{\parallel}$, we expect at finite magnetic field that the Landau-level energies $\hbar\omega_c(N+\frac{1}{2})$ will not enter the resonance condition. However, elastic impurity scattering inside the barrier can induce a coupling between the potential energy $E_{\perp}$ and the Landau-level energy during a tunneling process. In this case, transitions between different Landau levels will be allowed if the potential energy is changed by an integer multiple of the cyclotron energy $\hbar\omega_c$. For the 0-0 transition discussed here, the new resonance condition is given by

$$E_0^{\mathrm{inv}} = E_0^{\mathrm{acc}} + \Delta N \hbar\omega_c. \tag{3}$$

In Fig. 8(b), a tunneling process corresponding to the 0-0 transition is illustrated schematically for a magnetic field of $B = 5$ T, where the Landau-level index is changed by $\Delta N = 2$ at reverse bias. E denotes the total energy of an electron, which is still conserved. Note that tunneling is only possible if the target level is not completely occupied. The filling factors were calculated from the electron concentrations in the two 2D EG systems at $B = 0$ T, spin effects were neglected. To a good approximation, the electron densities in both the accumulation and the inversion channel can be assumed to be constant within a bias voltage range of $V_b = \pm 20$ mV. To achieve the situation plotted in Fig. 8(b), the applied bias voltage has to differ from the $E_0^{\mathrm{inv}} \rightarrow E_0^{\mathrm{acc}}$ resonance position by $\Delta V_b = -2\hbar\omega_c/e$. Tunneling can occur between the lowest Landau level in the accumulation layer, $\mathrm{LL}_0^{\mathrm{acc}}$, and the second Landau level in the inversion layer, $\mathrm{LL}_2^{\mathrm{inv}}$, as well as between $\mathrm{LL}_1^{\mathrm{acc}}$ and $\mathrm{LL}_3^{\mathrm{inv}}$, and so on. At higher magnetic fields, the Landau-level spacings and filling factors are different, but qualitatively the situation does not change.

In contrast to the 0-0 transition, tunneling processes into Landau levels of the higher subbands of the inversion channel are not resolved. As the energy differences between these subbands are considerably smaller than the spacing $E_1^{\mathrm{inv}} - E_0^{\mathrm{inv}}$, all expected features are probably washed out by the overlapping resonances and the exponentially growing contribution of nonresonantly tunneling electrons at more negative bias voltages.

As discussed above, scattering processes are necessary to induce tunneling between Landau levels with different indices. The low temperatures, at which the experiments are performed, ensure that interface roughness and impurity scattering are the dominant scattering mechanisms. To analyze the influence of impurity scattering in combined action with the magnetic field, the tunneling electrons can be described in a classical one-electron picture as a free carrier which moves in an external electric and magnetic field orientated parallel to each other. The diameter of the helix-type trajectory is given by the cyclotron radius $r_c = \sqrt{\hbar/m\omega_c}$, whereas the length is determined by the electric field and the transition time τ, respectively. Note that under our experimental conditions $\omega_c\tau \ll 1$ is always valid. Using the classical equations of motion, where the length s of the particle trajectory is given by $s = \int dt\,|\vec{v}(t)|$, a term proportional to $B\ln(\mathrm{const} \times \sqrt{1/B})$ has to be added to the $B = 0$ T tunneling distance. Since the length of the trajectory is enlarged by the magnetic field, the probability of an electron to be scattered inside the barrier increases as B grows larger. On the other hand, scattering processes are responsible for a coupling between the potential energy and Landau-level energy of an electron. As a consequence, tunneling between Landau levels with different indices becomes more probable at higher magnetic fields. This is reflected in the experimental data, as at fields above $B = 5$ T the amplitudes of the Landau-level–Landau-level tunneling peaks ($\Delta N \neq 0$) are comparable to the 0-0 subband resonance ($\Delta N = 0$).

In summary, we have investigated the tunneling processes between two fully quantized systems. Peaks in the derivative of the tunneling current were used to identify transitions between Landau levels with different indices on both sides of the barrier. These normally forbidden transitions are enabled by elastic scattering processes inside the $\mathrm{Al}_x\mathrm{Ga}_{1-x}\mathrm{As}$ barrier, thereby coupling the potential energy and the Landau-level energy. By analyzing intensities and linewidths of the magnetic-field-induced structures, it is demonstrated that apart from interface roughness, impurity scattering is the dominant mechanism breaking the expected conservation laws. At high magnetic fields, the amplitude of the Landau-level–Landau-level tunneling peaks is comparable to the subband resonances. In reverse bias, where electrons can be injected into higher Landau-levels of the inversion layer, a situation can be realized, where unoccupied Landau levels exist below the injection energy. Thus, Landau-level inversion could be obtained, which would be a promising mechanism to realize a tunable light source in the far-infrared spectral range.

IV. TUNNELING PROCESSES IN TRANSVERSE MAGNETIC FIELDS

Experiments in which a magnetic field is oriented parallel to the layers of the sample, i.e., perpendicular to the tunneling current, are discussed in this section. The results give detailed information about momentum and energy selection rules for 2D-2D electron tunneling. Again, the influence of an additional backgate voltage is investigated in order to confirm the obtained results.

The influence of transverse magnetic fields on electron tunneling was originally studied with Sb-doped germanium tunnel diodes, where an applied magnetic field caused a drastic decrease in the reverse tunneling current.[27] More recently, similar results were obtained for double-barrier heterostructures, where the reduction of the tunneling current was attributed to an increased effective barrier height.[28,29] In addition, with increasing magnetic field the minimum of the negative differential resistance was observed to shift to higher bias voltages.[30] When applied to 2D EG systems, a high transverse magnetic field leads to the formation of so-called magnetoelectric hybrid states or magnetoquantized interface states, since the magnetic- as well as the electric-potential contribution causes a confinement perpendicular to the interface. These states correspond to the classical skip-

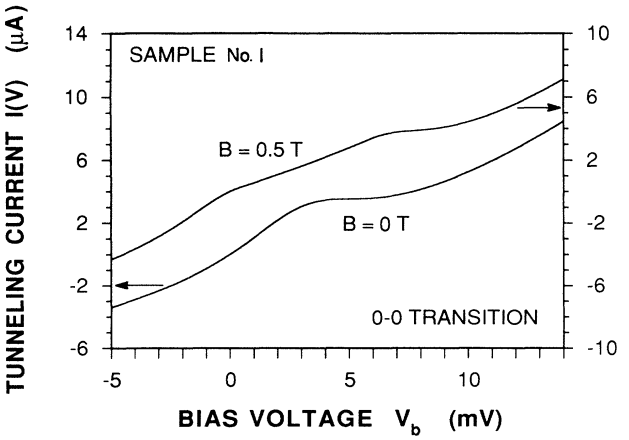

FIG. 9. Resonance broadening of the 0-0 transition in a tranverse magnetic field of $B = 0.5$ T, schematically shown for the current-voltage characteristics $I(V_b)$ of sample No. 1. The widths of the resonances are indicated by bars.

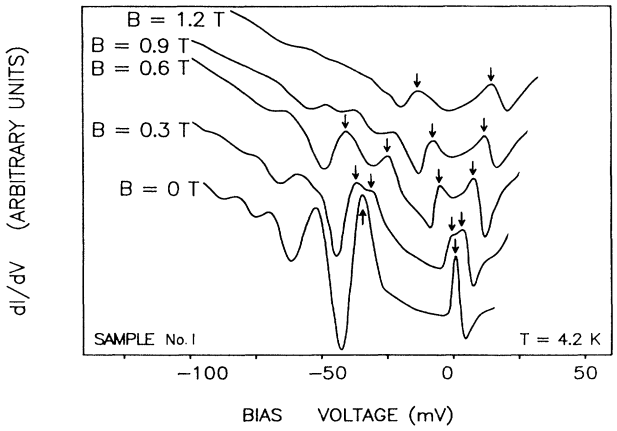

FIG. 10. dI/dV_b curves of sample No. 1 for various in-plane magnetic fields. The arrows indicate the splitting of the $B = 0$ T resonance peaks.

ping orbits, which describe the cyclotron movement along an interface. Experimentally, these states have been observed as a series of oscillations in d^2I/dB^2 (I is the tunneling current), in InP-$In_xGa_{1-x}As$ as well as in GaAs-$Al_xGa_{1-x}As$ single-barrier heterostructures.[31–33] In double barriers, tunneling transitions into magnetoelectric hybrid states were investigated at high transverse magnetic fields.[34,35] In this case, the region of negative differential resistivity becomes less pronounced as the magnetic field is increased.[36,37] In device research, a magnetic field transverse to the tunneling direction can be used to tune the electron's energy, for example, for studying the ballistic electron contribution to the $I(V_b)$ characteristic of vertically integrated resonant tunneling diodes.[38] To explain the observed effects, theoretical calculations have been performed on single-interface heterostructures and on (multi)quantum wells, leading to two main findings. First, the formation of magnetoelectric hybrid states results in an increase of the subband energies and the subband spacings[39–43] and also breaks the symmetry of the dispersion relation. Second, the magnetic field induces a change of the transverse momentum of the tunneling electrons due to the Lorentz force.[44–46] These two effects were found to be responsible for a new type of oscillation in the tunneling current characteristic between a (2D) accumulation layer and a (2D) wide quantum well.[47]

In our experiment, we investigate the influence of small transverse magnetic fields on the tunneling processes in order to obtain information about the momentum conservation rules. The steplike resonances in the current-voltage characteristic $I(V_b)$ broaden as the magnetic field increases and form a very weak double step structure. Figure 9 schematically shows a comparison between the narrow $B = 0$ T resonance structure and the broadened $B = 0.5$ T structure for the 0-0 transition of sample No. 1. The other transitions behave in a similar way. All current resonance structures rapidly become less pronounced for increasing magnetic field and totally vanish at magnetic fields $B > 2$ T. This effect is much better resolved in the derivative of the tunneling current dI/dV_b. Here, the drastic broadening of the resonances in the presence of a transverse magnetic field leads to a splitting of the dI/dV_b peaks into two small resonance peaks, marked by arrows for the 0-0 and the 0-1 transitions in Fig. 10. When the magnetic field grows larger, the intensity of the resonance peaks decreases rapidly. Although the effect of resonance broadening is also observable for higher transitions, the experimental data are very difficult to analyze as the structures in dI/dV_b are very weak and only of steplike appearance. Additionally, the overlap of the split peaks, as well as the spreading at high negative bias voltages, makes it complicated to identify all the features. It must be emphasized that the splitting is larger by one order of magnitude than the cyclotron energy $\hbar\omega_c$, which shows that the Landau levels are not responsible for this effect.

We first explain the observed effects within a quantum-mechanical picture. Subsequently, a simple classical picture is discussed, where the tunneling particle is understood as a free electron, the trajectory of which is determined by external forces due to the electric and magnetic field.

The calculations, which are based on the envelope function approximation, start with the potential distribution shown in Fig. 1(a). In order to study the influence of a transverse magnetic field on the subband energies and dispersion relations, the Schrödinger equation has to be solved for the complete system. To simplify the problem, we proceed from the potential $V(z)$ obtained by self-consistent calculations at $B = 0$ T. When a transverse magnetic field is applied to the sample, the kinetic momentum in the Schrödinger equation has to be replaced by $\mathbf{p} + e\mathbf{A}$. Choosing the magnetic field orientation in the x direction, the vector potential $\mathbf{A}$ in Landau gauge is $\mathbf{A} = (0, -Bz, 0)$. Consequently, the Hamilton operator depends on the z coordinate only, which leads, using the separation ansatz $\Psi_\nu(\mathbf{r}) = e^{ik_x x}e^{ik_y y}f_\nu(z)$, to the following equation for the conduction-band envelope function $f_\nu(z)$:

$$\left[\frac{\hbar^2 k_x^2}{2m(z)} + \frac{e^2B^2}{2m(z)}\left(z - \frac{\hbar k_y}{eB}\right)^2 - \partial_z \frac{\hbar^2}{2m(z)}\partial_z + V(z) - E_\nu(k_x, k_y)\right] f_\nu(z) = 0. \quad (4)$$

The spin of the electrons is not taken into account, since the magnetic fields are small. For further simplification, nonparabolicity effects are neglected assuming a constant effective mass $m(z) = m^*$. Therefore, the additive energy term $\hbar^2 k_x^2/2m^*$ is omitted in the following considerations. The in-plane magnetic field gives rise to the second term in Eq. (4), which is quadratic in z. For this parabolic potential contribution the center coordinate z_0 is defined as $z_0 = -\hbar k_y/eB$. To solve the problem numerically, the finite difference method is used, transforming the differential equation into an eigenvalue problem of the corresponding tridiagonal matrix. The subband energies (eigenvalues) and envelope functions (eigenvectors) are calculated using EISPACK algorithms for band matrices.[48] In doing so, the center coordinate z_0 or the momentum component k_y, respectively, are treated as a parameter, whereas k_x is set to zero. The resulting dispersion relations $E_\nu(z_0)$ of the lowest three subbands of our 2D-2D system are plotted in Fig. 11 for a fixed magnetic field of $B = 1$ T. The shape of the electric potential is marked by a dotted line.

We first discuss the limit of zero magnetic field: in the case of $B = 0$ T, the center coordinate z_0 is no longer defined. The term quadratic in z of Eq. (4) converges to $\hbar^2 k_y^2/2m^*$, only k_y is a valid parameter and, in addition, a good quantum number. For that reason, the dispersion relations of Fig. 11 turn into the simple analytic form $E_\nu(k_y) = E_\nu + \hbar^2 k_y^2/2m^*$, where E_ν denotes the energy of the νth subband edge. By applying a voltage to the sample, these parabolas are shifted in energy with respect to each other. Since a resonance position is achieved, if two subband edges are aligned, the dispersion parabola of a subband belonging to the inversion channel coincides completely with the dispersion parabola of a subband belonging to the accumulation layer. Thus, all electrons are allowed to tunnel resonantly, provided that final states are available. For nonzero magnetic field, the dispersion relations can be defined as a function of the wave-vector component k_y or as a function of the center coordinate z_0. Both representations are equivalent.

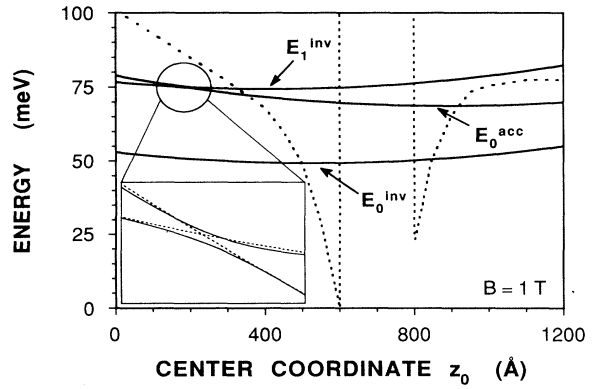

FIG. 11. Numerically calculated dispersion relations $E_0^{\rm inv}(z_0)$, $E_0^{\rm acc}(z_0)$, and $E_1^{\rm inv}(z_0)$ as a function of the center coordinate z_0 at a magnetic field of $B = 1$ T. The dotted line indicates the potential used in the calculations. The full lines represent the numerically obtained results, while the broken lines (framed inset) are calculated using perturbation theory. The inset's dimensions are 100 Å in the horizontal and 2 meV in the vertical direction, respectively.

A magnetic field in the x direction, however, breaks the symmetry between positive and negative k_y values because the energy depends on the center coordinate relative to the sample interface. As shown in Fig. 11 for $B = 1$ T, the dispersion relations $E_\nu(z_0)$ exhibit parabolic behavior near their minimum. The vertices are shifted horizontally with respect to each other. At the encircled point, where an intersection of the two dispersion relations $E_0^{\rm acc}(z_0)$ and $E_1^{\rm inv}(z_0)$ is expected, an anticrossing behavior is observed, as indicated inside the enlarged inset (full lines). The resulting energy gap, however, is very small ($\ll 0.2$ meV). Therefore, an electron having a wave vector k_y and energy $E_\nu(k_y)$ of such an intersection point is allowed to change its quantum-mechanical state satisfying the energy and momentum conservation rules. As long as the energy of this anticrossing point is below the Fermi level of one 2D system, then resonant tunneling is possible, even if the subband edges of the corresponding states are not exactly aligned in energy, but are shifted by $\Delta E_\perp$ with respect to each other. From Fig. 11 it is clear that positive as well as negative values are allowed for $\Delta E_\perp$, depending on which side of the $E_1^{\rm inv}(z_0)$ parabola's vertex the anticrossing point is situated. Consequently, the zero-field resonance condition (1) has to be replaced by

$$E_n^{\rm inv} = E_0^{\rm acc} + \Delta E_\perp. \quad (5)$$

Thus, resonant tunneling occurs at a bias voltage $V_b + \Delta V_b$, where $\Delta V_b = \Delta E_\perp/e$.

In order to determine the possible values of $\Delta E_\perp$ analytically, the dispersion relations were calculated using pertubation theory. This is a valid approximation, since at magnetic fields below $B = 3$ T wave functions and subband energies in the 2D systems are only weakly influenced by the occurrence of magnetoelectric hybrid states.[42] The analytic result is given by

$$E_\nu(z_0) = E_\nu + \frac{e^2B^2}{2m^*}(\langle z_\nu^2\rangle - \langle z_\nu\rangle^2) + \frac{e^2B^2}{2m^*}(z_0 - \langle z_\nu\rangle)^2. \quad (6)$$

The first term denotes the energy of the subband edge in case of zero magnetic field, the second one corresponds to the so-called diamagnetic shift. At a magnetic field of $B = 2$ T this constant shift is smaller by more than 2 orders of magnitude compared to E_ν, and is therefore neglected. The expectation values of the z coordinate and its square in the state $|\Psi_\nu\rangle$ are indicated by $\langle z_\nu\rangle$ and $\langle z_\nu^2\rangle$, respectively. The last term of the sum (6) is responsible for the dispersion, and can be written as

$$\frac{e^2B^2}{2m^*}(z_0-\langle z_\nu\rangle)^2=\frac{\hbar^2}{2m^*}\left(k_y-\frac{\langle z_\nu\rangle}{\ell^2}\right)^2, \tag{7}$$

where ℓ is the magnetic length, $\ell=\sqrt{\hbar/eB}$. From this equation it is obvious that, in first-order pertubation theory, the in-plane magnetic field causes the dispersion relation $E_\nu(z_0)$ to shift its vertex towards the expectation value of the z coordinate in real space, $\langle z_\nu\rangle$, of the corresponding quantum state. Both the numerically calculated results and the analytic results obtained by pertubation theory are plotted in Fig. 11. The only clear deviation is detectable in the encircled region, where numerical results show an anticrossing behavior (full lines), while the analytic curves intersect (broken lines). If the parabolas on each side of the barrier are shifted energetically by $\Delta E_\perp$ with respect to each other, the intersection point moves along both curves. Note that in this approximation the subband energies are assumed to be constant as the applied voltages are small. Using the analytic expressions for the parabolas (7), the center coordinate $z_{0,i}$ corresponding to the intersection point of the dispersion relations, for example, $E_0^{\rm acc}(z_0)$ and $E_n^{\rm inv}(z_0)$, is given by

$$\frac{e^2B^2}{2m^*}(z_{0,i}-\langle z^{\rm acc}\rangle)^2=\Delta E_\perp+\frac{e^2B^2}{2m^*}(z_{0,i}-\langle z_n^{\rm inv}\rangle)^2, \tag{8}$$

where $\Delta E_\perp$ denotes the difference in the vertex energy of both states. As resonant tunneling is no longer possible, if the energy of the intersection point exceeds the Fermi energy of the quantum state the electron starts from, i.e., $E_F^{\rm acc}$,[1] we can state that the value of $\Delta E_\perp$ is restricted to a well-defined range. At this point it must be emphasized that the Fermi energy does not change compared to the case of zero magnetic field, because the dispersion in k_y direction is only shifted in k space, according to Eq. (7). In order to determine the maximum resonant tunneling range, the center coordinates corresponding to the Fermi energy in the accumulation layer have to be calculated, leading to values of

$$z_{0,F}^{\rm acc}=\langle z^{\rm acc}\rangle\pm\left(\frac{2m^*E_F}{e^2B^2}\right)^{1/2}. \tag{9}$$

On the basis of these values, the maximum range of $\Delta E_\perp$ is given by

$$\Delta E_{\perp,n}^{\rm max}=-\left[\pm\left(\frac{2E_F}{eB}\right)^{1/2}(\langle z^{\rm acc}\rangle-\langle z_n^{\rm inv}\rangle)+\frac{e^2B^2}{2m^*}(\langle z^{\rm acc}\rangle-\langle z_n^{\rm inv}\rangle)^2\right]. \tag{10}$$

In our experiment, resonances for a fixed value of $\Delta E_\perp$ appear in the tunneling current at a shifted bias voltage $V_b+\Delta V_b$, where $\Delta V_b=\Delta E_\perp/e$. Therefore, the sharp zero-field resonances broaden to a wide but confined resonance range, which is clearly shown in Figs. 9 and 10. Assuming that the tunneling electrons lead to a constant current contribution within the resonance range, the steplike resonance structure in $I(V_b)$ is extended to a double steplike shape. Because of the exponential background due to the nonresonant tunneling electrons, this effect is very weak but observable, as shown in Fig. 9 in case of the 0-0 transition at a magnetic field of $B=0.5$ T. In the derivative of the tunneling current, the extension of the resonance condition results in a broadening and finally in a splitting of the zero-field dI/dV_b peaks. Both the onset and the end of the resonant tunneling regime are marked by a peak. The values of the bias voltage that correspond to the positions of the split peaks in dI/dV_b are plotted in Fig. 12(a) as a function of the applied transverse magnetic field. The splitting is clearly observed for the 0-0 and the 0-1 transitions. An assignment of the other resonance structures in dI/dV_b to transitions into higher subbands is difficult due to the overlap and the drastic spreading of the peaks at more negative bias voltages.

The quantum-mechanical predictions presented above are based on the conservation of momentum and energy during the tunneling process. In order to compare theory and experiment, the positions of the split peaks in dI/dV_b

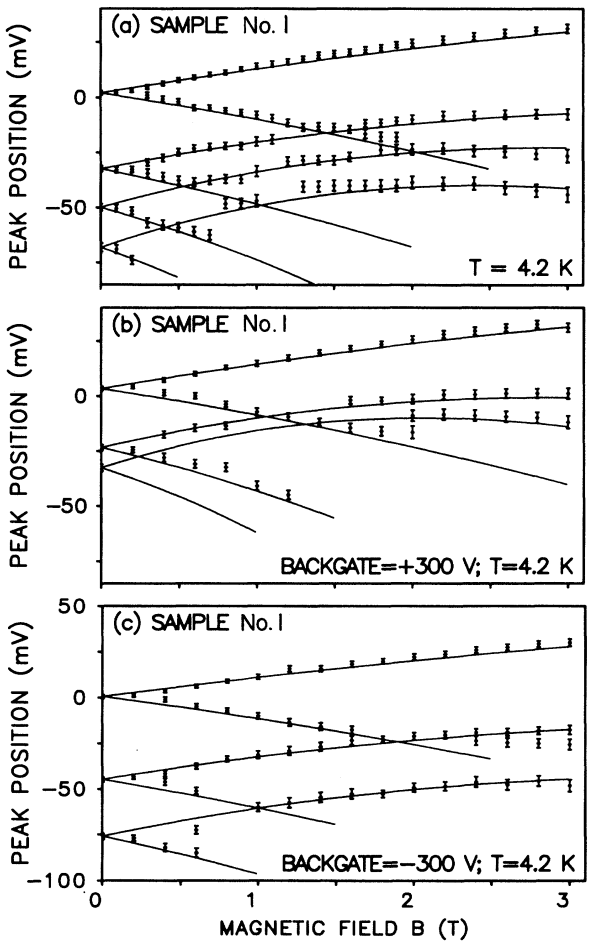

FIG. 12. Fan chart of the measured (dots with error bars) and theoretically calculated dI/dV_b peak positions, marking the maximum resonant tunneling range, at (a) zero backgate voltage; (b) an applied backgate voltage of $V_{\rm bg}=+300$ V; (c) an applied backgate voltage of $V_{\rm bg}=-300$ V.

are calculated, using Eq. (10). The Fermi energy used in this approximation is obtained by the self-consistent calculations performed at $B = 0$ T. Therefore, the dependence of E_F on the applied bias voltage V_b is included in this theory. The second important parameter is the distance $d_n = \langle z^{\rm acc}\rangle - \langle z_n^{\rm inv}\rangle$, which can classically be interpreted as the tunneling distance. Using the d values as a fitting parameter, it is possible to achieve an excellent agreement between experiment and theory, as shown in Fig. 12(a). The dots (error bars included) mark the positions of the split peaks, while the solid lines correspond to $\Delta V_b^{\rm max} = \Delta E_\perp^{\rm max}/e$. The d values giving the best fit are $d_0 = 350$ Å, $d_1 = 460$ Å, $d_2 = 570$ Å, and $d_3 = 650$ Å.

At low magnetic fields, the second term in Eq. (10) which is quadratic in B can be neglected, leading to the linear behavior evident in Fig. 12(a). If the magnetic field increases, this term becomes important and leads to the observed nonlinear behavior. In addition, the average distance between the mean value $\langle z_n^{\rm inv}\rangle$ and the GaAs-$Al_xGa_{1-x}As$ interface grows larger as the subband index increases. Therefore, the increase in the splitting of the resonance structures corresponding to the transitions into the higher subbands of the inversion channel can also be explained within this theory.

The mean values $\langle z^{\rm acc}\rangle$ and $\langle z_n^{\rm inv}\rangle$ are calculated self-consistently at conditions corresponding to the zero-field resonance positions. The calculations for low magnetic fields show that the influence of the magnetoelectric hybrid states on the mean values $\langle z_\nu\rangle$ and the Fermi energy can be neglected. Comparing d values obtained from the fit with the values determined theoretically ($d_0 = 340$ Å, $d_1 = 450$ Å, $d_2 = 540$ Å, and $d_3 = 610$ Å), excellent agreement is achieved. For the transitions into the lowest two subbands of the inversion channel the deviation between theory and experiment is only 10 Å; for the higher subbands the theory matches the experiment to within 40 Å. Note that, in principle, the d values depend on V_b, as the resonances are extended to a defined bias voltage range. This effect is mainly responsible for the deviation between theory and experiment for the transitions into the higher subbands of the inversion layer. In the case of the 0-0 and 0-1 transitions, however, the numerical results show only a small dependence on V_b, which cannot be resolved within the experimental accuracy. Therefore, the assumption of constant distances d_ν is justified when V_b is varied.

Using the fundamental assumption that canonical momentum and energy are conserved during the tunneling process, we are able to explain the experimental results within a very basic theory. The excellent agreement between calculated and experimental results further validates the mode used. The conservation of the momentum component parallel to the applied magnetic field, k_x, is obvious. If the magnetic field is applied parallel to the y direction, the symmetry of the problem implies that k_y is conserved. Therefore, in the case of zero magnetic field we conclude that both k_x and k_y are conserved, since the problem is symmetric with respect to the z direction. This is equivalent to the conservation of parallel momentum deduced from the results discussed in Sec. II of this paper.

The results obtained by tunneling spectroscopy in the presence of an in-plane magnetic field give information about both momentum and energy conservation rules, and also provide a powerful tool to determine the expectation values $\langle z_\nu\rangle$ of the states involved in electron tunneling. If the Fermi energy is known in the emitter electrode, the mean values $\langle z_\nu\rangle$ can be measured directly by fitting the experimental data according to the theory described above. This method holds advantages over methods such as capacitance measurements as the investigated subbands need not to be occupied. Additionally, the Fermi energy can be determined, if d_ν is known.

These experimental results can also be understood in terms of a classical picture. In this picture, the tunneling electron is regarded as a free particle with charge e and mass m^*, moving in crossed electric (z direction) and magnetic (x direction) fields. Classically, the Lorentz force couples the y and the z component of the momentum, which leads to a cycloidal trajectory. The z component Π_z of the kinetic momentum, however, is given by the potential energy of the electron in the initial state, $\Pi_z = \sqrt{2m^* E_\perp}/\hbar$. The subband energy $E_\perp$ is assumed to be independent of the applied magnetic field. For an electron tunneling through the barrier, the y component of the kinetic momentum is changed by

$$\Delta\Pi_y = -eB\Delta z/\hbar, \tag{11}$$

where Δz is the distance traveled in the z direction. Note that this is not in contradiction to quantum mechanics which states the conservation of the canonical momentum k_y, because the relation $\Pi_y = \hbar k_y$ is only valid in the case of zero magnetic field. The total energy of the starting electron is given by

$$E_\perp + \frac{\Pi_\parallel^2}{2m^*} = E_\perp + \frac{\Pi_x^2}{2m^*} + \frac{\Pi_y^2}{2m^*}. \tag{12}$$

The change in Π_y results in a change of Π_z by $\Delta\Pi_z$, corresponding to a change in $E_\perp$ by $\Delta E_\perp$. Therefore, the total energy beyond the barrier can be written as

$$E_\perp + \Delta E_\perp + \frac{\Pi_x^2}{2m^*} + \frac{(\Pi_y + \Delta\Pi_y)^2}{2m^*}. \tag{13}$$

Since the total energy must be conserved during the tunneling process, $\Delta E_\perp$ is evaluated as

$$\Delta E_\perp = [-2\Pi_y\,\Delta\Pi_y - (\Delta\Pi_y)^2]/2m^*. \tag{14}$$

As described above, $\Delta E_\perp$ is responsible for a shift of the zero-field resonance condition, similar to Eq. (5). Using the relation $E_F = \hbar^2\Pi_{y,F}^2/2m^*$, it turns out that Eqs. (14) and (10) are completely identical, if the tunneling distance Δz is replaced by the difference in mean values $d_n = \langle z^{\rm acc}\rangle - \langle z_n^{\rm inv}\rangle$.

This fact unambiguously shows the equivalence between the classical and quantum-mechanical picture. On the other hand, it can be concluded that the mean values $\langle z_\nu\rangle$ determine the tunneling distance, and not, as might be expected, the maximum of the local density, given by the maximum of $\langle \Psi_\nu^* \mid \Psi_\nu\rangle$.

Backgate voltage effects

In applying a backgate voltage V_{bg} to the sample, the electron density and the subband energies in the inversion channel can be changed, as discussed in Sec. II. Therefore it is possible to vary the mean distance of the electrons from one GaAs-$Al_xGa_{1-x}As$ interface, since the shape of the potential near this interface is strongly influenced by the depletion field. In order to confirm the results presented above, all tunneling measurements with in-plane magnetic field are repeated in the presence of an applied backgate voltage at values $V_{bg} = +300$ and -300 V. The experimental data are analyzed in the same way.

The results for $V_{bg} = +300$ V are shown in Fig. 12(b). As the depletion field at the lower interface (inversion channel) is reduced, only the transitions into the three lowest subbands are observed. At bias voltages below $V_b = -50$ mV, the structures are no longer resolved. As in the case of zero backgate voltage, the agreement between theory and experiment is very good. A comparison between the d values used to fit the measured data and the values obtained by the self-consistent calculations is shown in Fig. 13. The deviation is below 3%, which validates our assumptions concerning backgate voltage and transverse magnetic field. In the case of $V_{bg} > 0$, the envelope functions are more extended, which results in either a considerable increase of the d_ν values and thus the tunneling distance. Therefore, the fitted d values and the difference between the calculated expectation values are larger than in the case of zero backgate voltage. This, however, predicts a larger splitting at resonance, which is, in fact, observed.

In Fig. 12(c), the results for $V_{bg} = -300$ V are plotted. The resonance positions at zero magnetic field appear at much higher negative bias voltages, as the subband energies in the inversion layer increase due to the enhanced depletion field. In addition, a negative backgate voltage leads to a smaller average distance of the electrons from the lower GaAs-$Al_xGa_{1-x}As$ interface. Again it is possible to fit the experimental results very closely. The d values used in the fit and the self-consistently calculated differences in the expectation values are shown in Fig. 13. For the lowest two transitions, the deviation between theory and experiment is below 10 Å; for the 0-3 transition, theory matches the experiment within 30 Å. Note that the latter transition occurs at a comparatively high bias voltage. Therefore, the dependence of the d values on V_b can no longer be neglected. As the tunneling distance is reduced by a negative backgate voltage, the splitting is decreased as compared to the case of $V_{bg} = 0$ V.

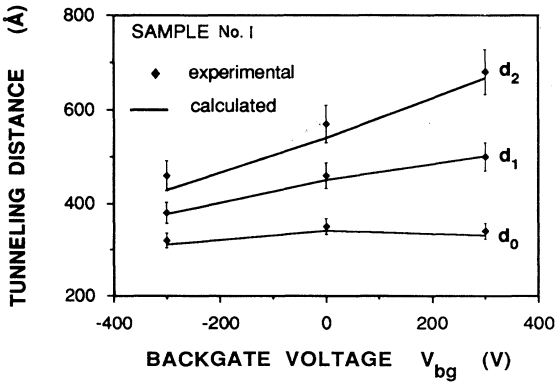

FIG. 13. Comparison between the d values obtained from the fits, denoted as experimental data (with 5% error bars), and the values determined by self-consistent calculations (solid lines) as a function of the applied backgate voltage.

All d values, whether they are obtained from fitting the experimental data (indicated by filled rhombs, including 5% error bars) or from self-consistent calculations (solid lines, denoted as theoretical data), are plotted in Fig. 13 as a function of the applied backgate voltage $V_{bg} = -300, \pm 0,$ and $+300$ V. In applying a backgate voltage to the sample, it is possible to vary the extension of the electronic states in the inversion channel within a large range. The broadening of the resonance range in the presence of an in-plane magnetic field, however, is very sensitive with respect to the expectation values of the z coordinate of the initial and the final state which are involved in the resonant tunneling process. As a result, transitions into the higher subbands of the inversion layer show the predicted behavior according to our theory discussed in Sec. II. The agreement between the experimental and calculated data further proves our interpretation of the resonance broadening.

In summary, we use an in-plane magnetic field to study the momentum and energy conservation rules for electron tunneling between two independently contacted 2D EG systems. In analyzing the magnetic-field-induced broadening of the sharp 2D-2D resonances, we are able to deduce that canonical momentum is conserved during tunneling. In addition, the parallel momentum $\mathbf{k}_\parallel$ is conserved in the case of zero magnetic field. The observed effects are explained within a quantum-mechanical picture based on pertubation theory as well as a classical picture based on the equations of motion of a charged particle in a crossed-fields configuration. We show that these two pictures are equivalent, if the difference between the expectation values of the states (subbands) which are involved in the tunneling process corresponds to the classical tunneling distance. It is also shown how the distances between the mean values of the wave functions on both sides of the barrier can be tuned within a large range through the application of a backgate voltage to the sample. Thus, it is possible to vary the tunneling distance d which determines the width of the resonance broadening. The influence of V_{bg} on the electron concentration can be neglected.

V. CONCLUSION

In this paper, we report on detailed studies of electron tunneling between two barrier-separated 2D EG systems. The resonances in the tunneling current are identified as transitions between quantized states on both sides of the barrier. The comparison between the experimental data and the theoretical results obtained by a self-consistent calculation show that a bias voltage V_b causes the 2D EG

levels to shift energetically by $\Delta E = eV_b$. Experiments with an additionally applied backgate voltage confirm this result.

Tunneling processes between Landau levels with different quantum numbers are observed in the case of a magnetic field applied perpendicular to the interfaces. We show that the selection rules for tunneling transitions break down for fields higher than $B = 3$ T. Due to scattering processes, the expected energy and momentum conservation laws no longer apply.

In the parallel field geometry, our tunneling experiment proves that canonical momentum is conserved during a tunneling process for a magnetic field lower than $B = 3$ T. The observed phenomena yield an elegant way to determine "tunneling distances."

In addition, such a heterostructure is ideally suited to study the influence of scattering processes on electron tunneling by performing temperature-dependent and tilted-field measurements.

ACKNOWLEDGMENTS

This work was partially sponsored by Bundesministerium für Forschung und Technologie via GAE-Verbundprojekt C2 (NT 2718 B).

[1] L. Esaki, Phys. Rev. **109**, 603 (1958).
[2] D. C. Tsui, Phys. Rev. Lett. **24**, 303 (1970).
[3] D. C. Tsui, Phys. Rev. B **4**, 4438 (1971).
[4] D. J. BenDaniel and C. B. Duke, Phys. Rev. **160**, 679 (1967).
[5] U. Kunze, J. Phys. C **17**, 5677 (1984).
[6] L. L. Chang, L. Esaki, and R. Tsu, Appl. Phys. Lett. **24**, 593 (1974).
[7] F. Hirler, J. Smoliner, E. Gornik, and G. Weimann, Appl. Phys. Lett. **57**, 261 (1990).
[8] E. E. Mendez, in *Physics and Applications of Quantum Wells and Superlattices*, edited by E. E. Mendez and K. von Klitzing (Plenum, New York, 1987), p. 159.
[9] T. Nakagawa, H. Imamoto, T. Kojima, and K. Ohta, Appl. Phys. Lett. **49**, 73 (1986).
[10] E. E. Mendez and L. L. Chang, in *EP2DS8 Proceedings of the Eighth International Conference of the Electronic Properties of Two-Dimensional Systems, Grenoble, France, 1989*, edited by J. Y. Marzin, Y. Guldner, and J. C. Maan [Surf. Sci. **229**, 173 (1990)].
[11] J. Smoliner, E. Gornik, and G. Weimann, Phys. Rev. B **39**, 12 937 (1989).
[12] J. Smoliner, W. Demmerle, G. Berthold, E. Gornik, G. Weimann, and W. Schlapp, Phys. Rev. Lett. **63**, 2116 (1989).
[13] W. Demmerle, J. Smoliner, G. Berthold, E. Gornik, G. Weimann and W. Schlapp, in *EP2DS8 Proceedings of the Eighth International Conference of the Electronic Properties of Two-Dimensional Systems, Grenoble, France, 1989* (Ref. 10), p. 169.
[14] R. Christanell and J. Smoliner, Rev. Sci. Instrum. **59**, 1290 (1988).
[15] P. J. Price, Phys. Rev. B **38**, 1994 (1988).
[16] R. Lassnig and W. Boxleitner, Solid State Commun. **64**, 979 (1987)
[17] F. Stern and S. Das Sarma, Phys. Rev. B **30**, 840 (1984).
[18] L. Hedin and B.I. Lundquist, J. Phys. C **4**, 2064 (1971).
[19] R. Lassnig, Phys. Rev. B **31**, 8076 (1985).
[20] J. Smoliner, R. Christanell, M. Hauser, E. Gornik, G. Weimann, and W. Schlapp, Appl. Phys. Lett. **50**, 1727 (1987).
[21] J. Smoliner, E. Gornik, and G. Weimann, Appl. Phys. Lett. **52**, 2136 (1988).
[22] T. W. Hickmott, Solid State Commun. **63**, 371 (1987).
[23] E. E. Mendez, L. Esaki, and W. I. Wang, Phys. Rev. B **33**, 2893 (1986).
[24] C. E. T. Gonçalves da Silva and E. E. Mendez, Phys. Rev. B **38**, 3994 (1988).
[25] L. Eaves, E. S. Alves, M. Henini, O. H. Huges, M. L. Leadbeater, C. A. Payling, F. W. Sheard, G. A. Toombs, A. Celeste, J. C. Portal, G. Hill, and M. A. Pate, in *Proceeedings of the International Conference on the Application of High Magnetic Fields in Semiconductor Physics, Würzburg, Germany, 1988,* Springer Series in Solid State Science Vol. 87 (Springer-Verlag, Berlin, 1989), p. 324.
[26] B. E. Kane, D. C. Tsui, and G. Weimann, Phys. Rev. Lett. **61**, 1123 (1988).
[27] H. Roth, W. Bernard, W. D. Sraub, and J. E. Mulhern, Jr., Phys. Rev. **145**, 667 (1966).
[28] L. Eaves, K. W. H. Stevens, and F. W. Sheard, in *Physics and Fabrication of Microstructures and Devices*, Springer Proceedings in Physics Vol. 13 (Springer-Verlag, Berlin, 1986), p. 343.
[29] P. Guéret, A. Baratoff, and E. Marclay, Europhys. Lett. **3**, 367 (1987).
[30] E. E. Mendez, L. Esaki, and W. I. Wang, Phys. Rev. B **33**, 2893 (1986).
[31] B. R. Snell, K. S. Chan, F. W. Sheard, L. Eaves, G. A. Toombs, D. K. Maude, G. Hill, J. C. Portal, S. J. Bass, P. Claxton, and M. A. Pate, Phys. Rev. Lett. **59**, 2806 (1987).
[32] K. S. Chan, L. Eaves, D. K. Maude, F. W. Sheard, B. R. Snell, G. A. Toombs, E. S. Alves, J. C. Portal, and S. Bass, Solid State Electron. **31**, 711 (1988).
[33] J. A. Lebens, R. H. Silsbee, and S. L. Wright, Phys. Rev. B **37**, 10 308 (1988).
[34] E. S. Alves, M. L. Leadbeater, L. Eaves, M. Henini, O. H. Hughes, A. Celeste, J. C. Portal, G. Hill, and M. A. Pate, Superlatt. Microstruct. **5**, 527 (1989).
[35] L. Eaves, E. S. Alves, T. J. Foster, M. Henini, O. H. Hughes, M. L. Leadbeater, F. W. Sheard, G. A. Toombs, K. Chan, A. Celeste, J. C. Portal, G. Hill, and M. A. Pate, in *Physics and Technology of Submicrometer Structures*, edited by G. Bauer, F. Kuchar, and H. Heinrich, Springer Series in Solid State Sciences Vol. 83 (Springer-Verlag, Berlin, 1988), p. 74.
[36] M. L. Leadbeater, L. Eaves, P. E. Simmonds, G. A. Toombs, F. W. Sheard, P. A. Claxton, G. Hill, and M. A. Pate, Solid State Electron. **31**, 707 (1988).
[37] S. BenAmor, K. P. Martin, J. L. L. Rascol, R. J. Higgins, A. Torabi, H. M. Harris, and C. J. Summers, Appl. Phys.

Lett. **53**, 2540 (1988).
[38] J. J. L. Rascol, K. P. Martin, R. E. Carnahan, R. J. Higgins, L. Cury, J. C. Portal, B. G. Park, E. Wolak, K. L. Lear, and J. S. Harris, Jr. (unpublished).
[39] W. Zawadski, Semicond. Sci. Technol. **2**, 550 (1987).
[40] B. Huckenstein and R. Kümmel, Z. Phys. B **66**, 475 (1987).
[41] G. M. G. Oliveira, V. M. S. Gomes, A. S. Chaves, J. R. Leite, and J. M. Worlock, Phys. Rev. B **35**, 2896 (1987).
[42] V. M. S. Gomes, G. M. G. Oliveira, J. L. Leite, and A. S. Chaves, Superlatt. Mircrostruct. **6**, 47 (1989).
[43] M. P. Stopa and S. Das Sarma, Phys. Rev. B **40**, 10 048 (1989).
[44] L. Brey, G. Platero, and C. Tejedor, Phys. Rev. B **38**, 9649 (1988).
[45] J. K. Jain, and S. Kivelson, Phys. Rev. B **37**, 4111 (1988).
[46] F. Ancilotto, J. Phys. C **21**, 4657 (1988).
[47] M. Helm, F. M. Peeters, P. England, J. R. Hayes, and E. Colas, Phys. Rev. B **39**, 3427 (1989).
[48] B. S. Garbow, J. M. Boyle, J. J. Dongara, and C. B. Moler, in *Matrix Eigensystem Routines - EISPACK Guide Extension*, edited by G. Goss and J. Hartmanis, Lecture Notes in Computer Science Vol. 51 (Springer-Verlag, New York, 1977).